

## Highly tunable topological system based on PbTe-SnTe binary alloy

Cheng-Long Zhang <sup>1,\*</sup>, Tian Liang<sup>1,\*</sup>, Naoki Ogawa,<sup>1,2,3</sup> Yoshio Kaneko,<sup>1</sup> Markus Kriener <sup>1</sup>, Taro Nakajima,<sup>1,5</sup> Yasujiro Taguchi,<sup>1</sup> and Yoshinori Tokura<sup>1,2,4</sup><sup>1</sup>RIKEN Center for Emergent Matter Science (CEMS), Wako 351-0198, Japan<sup>2</sup>Department of Applied Physics, University of Tokyo, Tokyo 113-8656, Japan<sup>3</sup>PRESTO, Japan Science and Technology Agency (JST), 332-0012, Kawaguchi, Japan<sup>4</sup>Tokyo College, University of Tokyo, Tokyo 113-8656, Japan<sup>5</sup>Institute for Solid State Physics, The University of Tokyo, Kashiwa, Chiba 277-8561, Japan

(Received 8 June 2020; accepted 1 September 2020; published 22 September 2020)

Topological semimetals have been attracting great interest for their superb potentials. While many theoretical and experimental investigations have been performed for topological semimetals, their materials platform is still in demand. Here, we report a highly tunable materials system for topological semimetal, indium (In)-doped  $\text{Pb}_{1-x}\text{Sn}_x\text{Te}$ . By exploring the crystals with varying Pb/Sn ratios and In doping levels, a phase formation with low carrier concentration, high mobility, and large anomalous Hall effect is found for a finite area of the composition between topological crystalline insulator and normal insulator at ambient pressure. Furthermore, the in-plane anomalous Hall effect as a hallmark of Berry-curvature generation is also observed at low temperatures, where optical second-harmonic generation reveals the breaking of inversion symmetry. These results show that there is a finite range of topological semimetal phase in the PbTe-SnTe binary alloy, providing a promising materials platform to investigate the versatile nature of topological semimetals.

DOI: [10.1103/PhysRevMaterials.4.091201](https://doi.org/10.1103/PhysRevMaterials.4.091201)

The concept of topology as exemplified by the Thouless-Kohmoto-Nightingale-den Nijs formula [1] has developed into one of the most important notions in modern condensed matter physics. The last decade has witnessed an explosion of theoretical and experimental developments on topological phases of matter [2–5], including topological semimetals such as Dirac/Weyl semimetals (DSMs/WSMs) or nodal line semimetals (NLSMs). First-principles band calculations have achieved great success in predicting the stable DSMs such as  $\text{Cd}_3\text{As}_2$ ,  $\text{Na}_3\text{Bi}$  [6,7] and WSMs such as TaAs [8,9]. The speed of new topological materials discovery has recently been greatly accelerated by the advent of topological quantum chemistry [10] and developments of calculation codes based on symmetry analysis [11–14]. Nevertheless, an ideal, experimentally tunable material platform of topological semimetal is still missing for the exploration of versatile magneto/opto-/thermo-electronic properties and functions. This motivated us to pay more attention to the general theoretical prediction by Murakami and coworkers [15–19] (hereafter, we refer to this as Murakami's scheme) made more than a decade ago shortly after the theoretical prediction of topological insulator and its experimental realization in a form of a quantum well [20,21]. In Murakami's scheme, topological semimetals such as WSMs or NLSMs are theoretically predicted to arise naturally in inversion symmetry broken systems, as the intermediate phase connecting the normal insulator (NI) and the topological insulator or topological crystalline insulator (TCI)

phases. In light of the two control axes in the universal phase diagram of Murakami's scheme, i.e., the strength of inversion symmetry breaking versus the external control parameters such as lattice constant, pressure or composition, the presently investigated binary system, PbTe-SnTe with inherent ferroelectric instability [22,23], provides a good arena in which a topological semimetallic phase sandwiched by NI (PbTe) and TCI (SnTe) [24,25] can be explored.

The PbTe-SnTe system has been investigated due to its topological surface state and superconducting properties induced by In doping [26]. A recent work [27] reports that the PbTe-SnTe binary alloy system can be tracked to exhibit the topological phase transition by applying external pressure, with the topological semimetallic phase sandwiched by two insulating phases, being reminiscent of Murakami's scheme. However, the requirement of applying pressure to reach the topological semimetallic phase puts large practical technical constraints to perform further studies such as spectroscopic and thermal-transport measurements. This urged us to delicately design the PbTe-SnTe binary system, by finely changing the indium doping level as well as Pb/Sn ratio, to realize the possible topological semimetallic phase by controlling the chemical potential at ambient pressure. As described below, an intermediate phase with enhanced mobility, large Berry-curvature induced anomalous Hall effect, and [100]-oriented electronic polarization, is identified. Moreover, a large in-plane anomalous Hall effect is also observed in this intermediate phase, manifesting the emergence of a topological semimetallic phase.

The solid solution  $\text{Pb}_{1-x}\text{Sn}_x\text{Te}$  with rocksalt structure consists of the two end compounds, PbTe and SnTe, which are NI and TCI [28,29] respectively. Figure 1(b) sketches the

\*These authors contributed equally to this work.

†Corresponding author: [chenglong.zhang@riken.jp](mailto:chenglong.zhang@riken.jp)‡Corresponding author: [tian.liang@riken.jp](mailto:tian.liang@riken.jp)

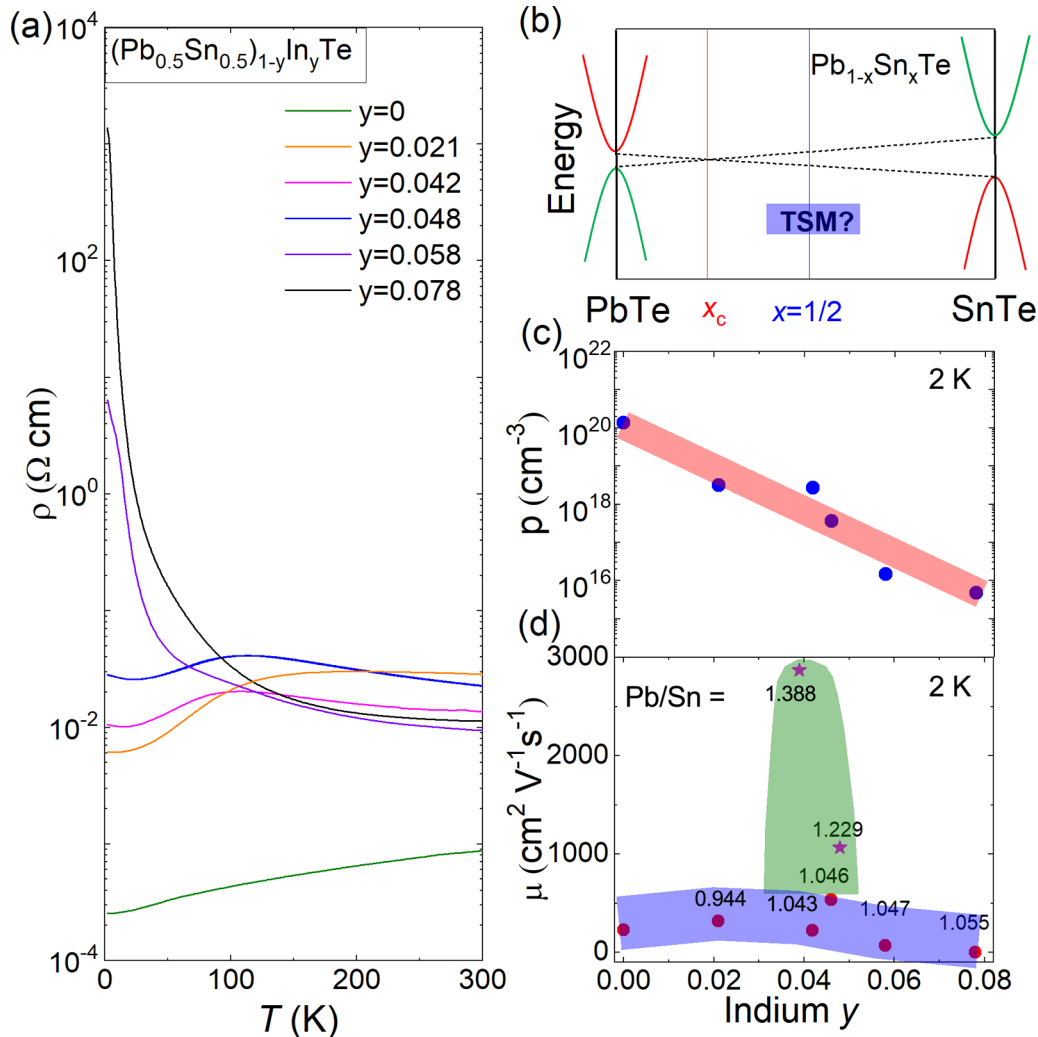


FIG. 1. Electrical transport properties of In doped  $(\text{Pb}_{0.5}\text{Sn}_{0.5})_{1-y}\text{In}_y\text{Te}$ . (a) Temperature-dependent resistivity of samples with different In doping concentrations. (b) Schematic phase diagram for the band evolution between normal insulator (NI;  $\text{PbTe}$ ) and topological crystalline insulator (TCI;  $\text{SnTe}$ ). By In doping for reducing the carrier density, topological semimetallic (TSM) features are expected to show up. (c) Hole-type carrier concentration  $p$  (2 K) plotted against In concentration. (d) Mobility  $\mu$  (2 K) plotted with respect to In concentration  $y$  for nominal Pb/Sn ratio of 1 ( $x = 0.5$ ). The analyzed Pb/Sn ratios are shown for each sample. Samples with actual Pb/Sn ratios within  $1.00 \pm 0.06$  are in the violet region. Only samples with Pb/Sn ratios off unity exhibits a large enhancement of  $\mu$  (indicated by the green area).

schematic band evolution of the  $\text{PbTe}$ - $\text{SnTe}$  binary system [29]. When inversion symmetry is preserved, the critical composition of  $x_c$  characterizing the transition point of the band inversion is predicted to be  $\sim 0.35$  in form of  $\text{Pb}_{1-x}\text{Sn}_x\text{Te}$  [30]. The goal is to incorporate inversion symmetry breaking by polar distortion inherent to the rocksalt-type tellurides to produce the topological semimetal phase, according to Murakami's scheme.

The initial target materials are  $(\text{Pb}_{1-x}\text{Sn}_x)_{1-y}\text{In}_y\text{Te}$ , with nominal values  $x = 0.5$  and  $y = 0, 0.02, 0.04, 0.06, 0.08$ . For  $x = 0.5$ ,  $y = 0.06$ , a crystal rod with a length of  $\sim 60$  mm was obtained (other compounds with different compositions are  $\sim 20$  mm in length). Those single crystals of  $(\text{Pb}_{1-x}\text{Sn}_x)_{1-y}\text{In}_y\text{Te}$  were grown by the conventional Bridgman-Stockbarger technique by adopting a procedure reported in the literature [27] (for details, see Ref. [31]). On the basis of the promising results obtained, we furthermore made three single crystal rods ( $\sim 60$  mm in length) with nominal

values of  $(x, y) = (0.25, 0.01), (0.43, 0.06),$  and  $(0.43, 0.04)$ . After cleavage, the rod was examined by powder x-ray diffraction ( $\text{Cu } K_\alpha$  at room temperature) and Laue reflection for checking its single-crystallinity and crystal orientation. Rods of mixed crystals, typically 60 mm in length, are expected to show a composition spread or gradient along the growth direction due to the well-known monotectoid tendency for the Bridgman-method growth of mixed crystals. For a more detailed characterization, the rod was cut into segments of 3 mm in length to check the stoichiometry by energy-dispersive x-ray spectroscopy (EDX). The peaks of indium (In) could be identified and separated from the adjacent tin (Sn) peaks in the EDX spectra. One piece of sample was also checked by inductively coupled plasma atomic-emission spectroscopy, which gave an indium value almost identical to the one measured by EDX. Electrical transport measurements were performed in a Quantum Design physical property measurement system (PPMS-9 T). A standard four-probe method

by using silver paste for contacts (with typical contact size of  $\sim 0.1$  mm) was adopted. All the samples were cut into thin plates and polished down to 0.03 mm in thickness, for transport measurements. Optical second harmonic generation (SHG) was measured with a pulsed laser source (120 fs, 1.55 eV) at normal incidence on the *ab* plane to examine the inversion symmetry breaking. The polarization of the laser was controlled by a half-wave plate, while that of the reflection SH signal was analyzed by a Glan-laser prism.

As shown in Fig. 1(a), the temperature dependence of resistivity for six selected samples with an EDX-characterized Pb/Sn ratio around unity ( $x \sim 0.5$ ) shows a systematic change from metalliclike ( $10^{-4}$   $\Omega$  cm at 2 K) to insulatinglike features ( $10^3$   $\Omega$  cm at 2 K) by increasing the In doping level. Indium is a so-called valence-skipping element [32–34], and this feature is often exploited when doping into these chalcogenide systems. In the current case, In doping (*y*) into  $\text{Pb}_{1-x}\text{Sn}_x\text{Te}$  reduces the bulk (hole-type) carrier number effectively. Therefore, doped In in this range of *y* nominally takes its 3+ state. The carrier concentrations estimated from Hall measurements for these six samples (Pb/Sn  $\sim 1$ ) are plotted against the In concentration *y* in Fig. 1(c). The sample without indium doping exhibits a hole-type carrier concentration as high as  $1.35 \times 10^{20}$   $\text{cm}^{-3}$ . By contrast, the most insulating sample shows a value as low as  $4.78 \times 10^{15}$   $\text{cm}^{-3}$ ; i.e., almost five orders of magnitude reduction of the carrier concentration can be achieved by In doping, revealing a good tunability of this system.

In the process of characterization, we found, while anticipated beforehand, that the chemical compositions of the elements of the as-grown crystals, especially the Pb/Sn ratio, are not uniform along the growth direction and differs from the nominal values, and that the transport and optical properties are found to be very sensitive to the variation of the compositions. As shown in Fig. 1(d), the samples with Pb/Sn ratio off unity (the green area) exhibit a large enhancement in electrical mobility up to  $\sim 2900$   $\text{cm}^2 \text{V}^{-1} \text{s}^{-1}$ , and are in sharp contrast with those with a Pb/Sn ratio around unity (shown in purple) with mobilities below  $500$   $\text{cm}^2 \text{V}^{-1} \text{s}^{-1}$ . Furthermore, as it will turn out to be clear (see the description below), while In does reduce the carrier density effectively, the appearance of electric polarity critically depends not only on the carrier density, but also on the Pb/Sn ratio.

For a more exact profile of the green area in Fig. 1(d), long ( $\sim 60$  mm) crystal rods, with nominal values of  $(x, y) = (0.5, 0.06)$ ,  $(0.25, 0.01)$ ,  $(0.43, 0.06)$ , and  $(0.43, 0.04)$ , were investigated to amplify the composition-spread effect along the growth direction. As shown in Figs. 2(a) and 2(b), a typical sample with nominal values of  $x = 0.5$  and  $y = 0.06$  was cut into 11 pieces and each piece was characterized by EDX. The overall In concentration is around 0.04 and changes only moderately along the growth direction. However, the Pb/Sn ratio varies with a trend of shifting to the Pb-rich side. As reported in Refs. [35–37], it is known that the insulating samples by In doping favor a nonequilibrium conducting state, in a finite range of Pb/Sn ratio ( $x \sim [0.22, 0.28]$ ), under light irradiation at room temperature. All the insulating samples we investigated in this paper are out of this range. We have checked one insulating sample with  $x \sim 0.3$  and found no discernible effect on resistivity versus temperature

curve even when light was irradiated at room temperature. The corresponding carrier concentration and mobility (2 K) of each piece of sample is shown in Figs. 2(c) and 2(d). Surprisingly, a higher-mobility ( $> 10^3$   $\text{cm}^2 \text{V}^{-1} \text{s}^{-1}$ ) region is located within a small area spanned by In concentration and Pb/Sn ratio. To fully map out the hot-spot of the phase diagram on a plane spanned over In and Pb concentrations, the same analysis was applied to three additional crystal rods with  $(x, y) = (0.25, 0.01)$ ,  $(0.43, 0.06)$ , and  $(0.43, 0.04)$  (see Ref. [31]). All the results are summarized in contour maps as shown in Figs. 2(e) and 2(f). Apparently, the system can be tuned to very high mobility and low carrier concentration within a small area in spite of this heavily mixed character of the solid solution (Pb,Sn,In)Te. Since interesting physical properties characteristic of topological semimetal phase are often achieved with low carrier concentration and enhanced mobility [27], the shaded pink regime, i.e., the composition range  $0.38 < x < 0.42$  and  $0.029 < y < 0.041$  in  $(\text{Pb}_{1-x}\text{Sn}_x)_{1-y}\text{In}_y\text{Te}$ , defines an initial target area where to look for possible topological semimetal phase.

Detailed investigation of charge transport and optical properties were performed on these crystals. We exemplify three typical samples, S33 [ $(x, y) = (0.48, 0.047)$ ], S35 (0.42,0.039), S40 (0.41,0.048) in some detail below (see Ref. [31] for the details of the other samples). Figure 3 summarizes the temperature dependence of resistivity  $\rho$ , hole carrier density *p* and mobility  $\mu$  of S33, S35, and S40. As shown in Figs. 3(a)–3(c), samples S33 and S35 exhibit a reentrant insulator-semimetal-insulatorlike transition. Sample S40 shows a narrow-gap intrinsic semiconductorlike feature and is insulating with resistivity values of the order of  $10$   $\Omega$  cm at low temperatures. This also concurs with the reduction of the carrier concentration by almost four orders of magnitude upon cooling. Only sample S35 exhibits a large mobility enhancement below 100 K, reaching approximately  $3000$   $\text{cm}^2 \text{V}^{-1} \text{s}^{-1}$  at 2 K, even though the carrier concentration is reduced by two orders of magnitude as compared to room temperature.

The above features signal that something unconventional may be happening in sample S35 and suggests to consider the possibility for emergence of topological semimetal phase sandwiched by NI and TCI phases according to Murakami's scheme. Since inversion symmetry breaking serves as an important tuning parameter in Murakami's scheme, the existence of the polar distortion is explored first. The end compound, SnTe, is known to be ferroelectric [38]. However, the existence of a ferroelectric distortion in the PbTe-SnTe alloy system remains elusive from the available literature so far. A recent study employing the modified Sawyer-Tower method reports a large spontaneous dielectric response at low temperatures [27]. However, measurements based on the modified Sawyer-Tower method requires a highly insulating sample (e.g., with the resistivity exceeding  $10^4$   $\Omega$  cm [27]) from a practical technical point of view, which is not suitable for the samples in our study. Here, we performed the SHG measurement on the selected samples to examine the inversion symmetry breaking. Among three samples (S33, S35, and S40), only S35 exhibits the detectable SH signal, while the other two samples give only polarization- and temperature-independent background signal. As shown in the

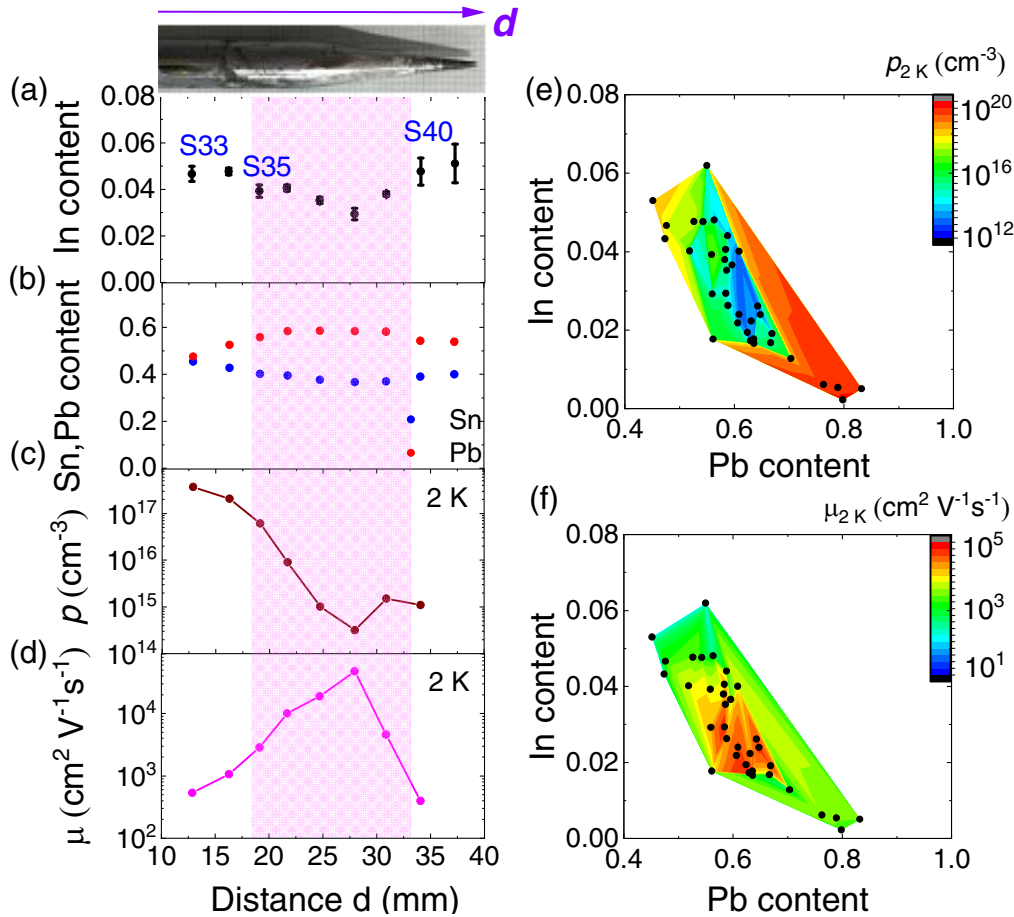


FIG. 2. Charge-transport characterization of single crystals  $(\text{Pb}_{1-x}\text{Sn}_x)_{1-y}\text{In}_y\text{Te}$  prepared with various compositions of Pb/Sn and In. (a)–(d) Position-dependent composition characterization of a long single crystalline rod with the nominal values of  $x = 0.5$ ;  $y = 0.06$ . Concentrations of (a) In  $y$ , (b) Sn  $x(1 - y)$ , and Pb  $(1 - x)(1 - y)$  determined by EDX (see text), (c) hole-type carrier concentration  $p(2\text{ K})$  and (d) mobilities  $\mu(2\text{ K})$  characterized piece by piece along the growth direction of the single crystalline rod shown on top of panel (a). The sample position is defined as the distance  $d$  measured from the top position of the as-grown crystal rod. The reddish area indicates the intermediate range of the crystal pieces exhibiting enhanced mobility values. (e) Hole-type carrier concentration  $p(2\text{ K})$  of all the samples from different crystal rods (including some rods with a Pb/Sn ratio larger than 1) The contour map is spanned by concentrations of In  $y$  and Pb  $(1 - x)(1 - y)$ . (f) The corresponding mobilities  $\mu(2\text{ K})$  of all these samples are summarized in the contour map.

SHG polarimetry [inset of Fig. 4(e)], the polar axis is found to be along [100], which is different from the previously assumed [111] direction [27]. The observed inversion symmetry breaking via temperature-dependent polar distortion, is reminiscent of Murakami’s scheme to produce the topological semimetal state.

To further characterize the electronic states, detailed charge transport measurements were performed. As shown in Fig. 4(a)–4(c), S33 and S40 exhibit a normal  $H$ -linear out-of-plane ( $H \parallel c$ ) Hall resistivity at low temperatures. However, the intermediate phase (S35) features a large anomalous Hall effect for the out-of-plane magnetic field, which displays the obvious steplike shape at fields exceeding  $\sim 3$  T, signaling the effect of Berry curvature generated in the topological semimetal phase. This anomalous Hall effect (AHE) appearing in such a nonmagnetic material is a field-induced AHE, and is different from that in ferromagnets. At zero magnetic field, the sources of the Berry curvature distribute in such a way that cancels out the total Hall signals, as required by time reversal symmetry (TRS) in case of a nonmagnetic material.

Once the magnetic field is turned on and TRS is broken, the sources of Berry curvature redistribute due to the Zeeman effect, allowing the AHE to appear at finite fields. We extracted the Hall carrier concentration from the initial slope of the Hall curve where the effect of Berry curvature contributed term is small. This observation is further corroborated by the in-plane Hall measurements. As shown in the inset of Fig. 4(a), the current and magnetic field are applied along the  $a$  and  $b$  directions, respectively, which means that the magnetic field and current lie in the same  $ab$  plane where electrical Hall contacts are placed (see Ref. [31] for technical details of the in-plane Hall measurements). When the magnetic field is applied in-plane, the conventional Lorentz force dies out, so that the conventional trivial Drude Hall signals vanish in the in-plane geometry. In other words, the sole contribution to the Hall signals in the in-plane geometry purely comes from the Berry curvature [39]. In the experiments, we detected in-plane anomalous Hall signals with Hall angle as large as  $\sim 0.04$ , manifesting the existence of the Berry curvature. The observed in-plane anomalous Hall conductivity can be

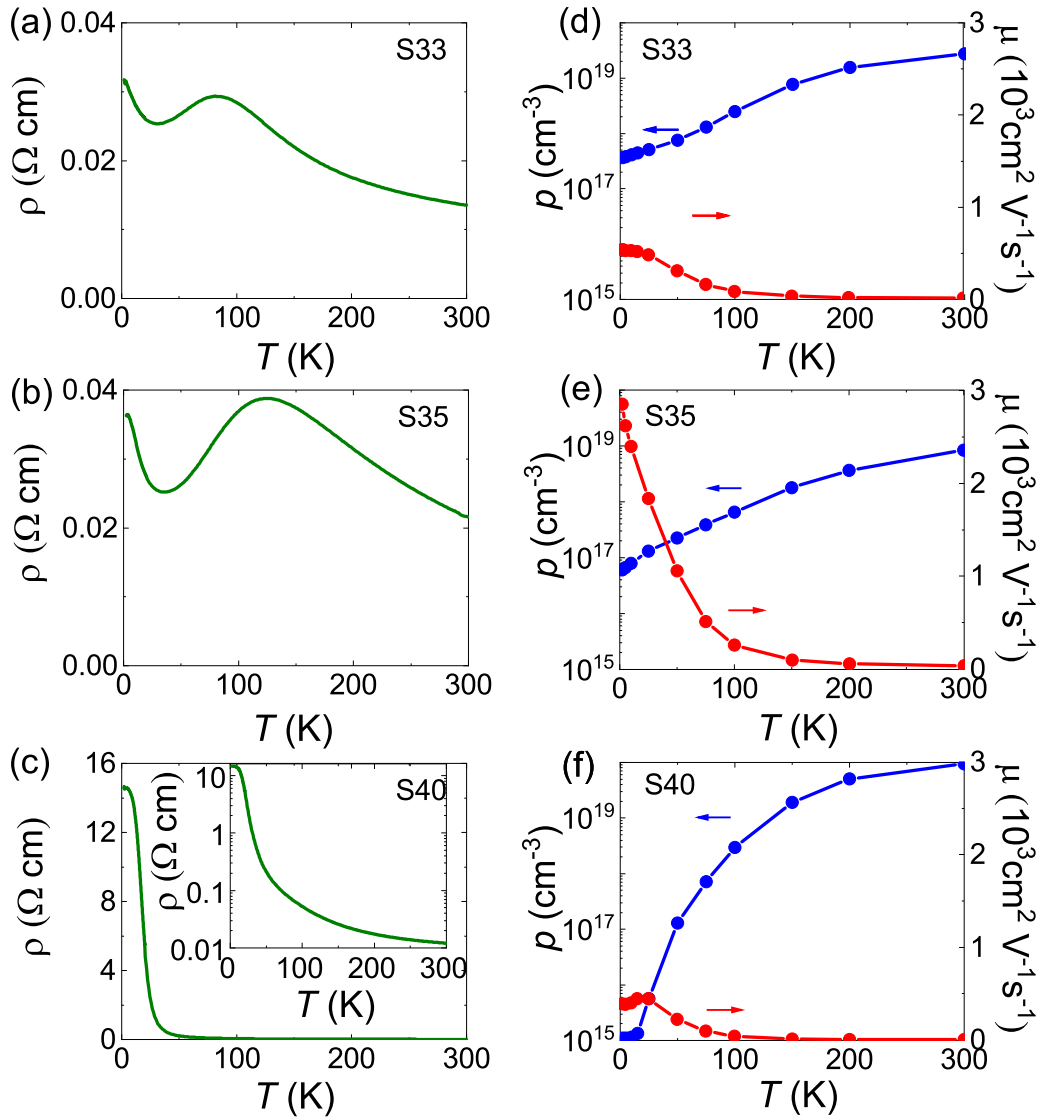


FIG. 3. Temperature dependence of charge transport properties on the three representative samples with slightly different compositions. (a)–(c) Temperature dependence of resistivity  $\rho$  for the three typical samples, S33, S35, and S40 [see Figs. 2(a) and 2(b)] for their accurate compositions. S33 and S35 exhibit semimetallic features at low temperatures. The inset of panel (c) shows a logarithmic-scale resistivity versus temperature, signifying the insulating behavior in sample S40. (d)–(f) Temperature dependence of carrier concentration  $p$  (blue lines) and mobility  $\mu$  (red lines). S35 exhibits a large enhancement of mobility below 100 K.

expressed as the integral of Berry curvature in the Brillouin zone [27], i.e.,

$$\sigma_{xy}^{\text{AHE}} = \frac{e^2}{\hbar} \int \frac{dk}{(2\pi)^3} \Omega_z(k) f_k^0 = e \cdot \frac{e}{\hbar} \langle \Omega_z \rangle p, \quad (1)$$

where  $f_k^0$  is the Fermi-Dirac distribution,  $\langle \Omega_z \rangle$  is the averaged Berry curvature over the occupied states in the Brillouin zone, and  $p$  is the total carrier density. Only the intermediate phase of S35 shows a pronounced in-plane ( $H \parallel \mathbf{b}$ ) anomalous Hall effect generated by Berry curvature, while the in-plane Hall signals of S33 and S40 are vanishingly small. This is because in S33 and S40, the inversion symmetry is preserved and hence there is no source to generate the Berry curvature, in stark contrast to sample S35, which is identified as a topological semimetal.

Finally, the in-plane Hall signals are measured as a function of temperature to quantify the evolution of the Berry curvature. The Berry curvature  $\langle \Omega_z \rangle \propto \sigma_{xy}^{\text{in-plane}}/p$  is negligible at temperatures higher than 100 K, but greatly enhanced below, as shown in Fig. 4(e), in accord with the temperature evolution of mobility of this crystal [Fig. 3(e)]. This observation indicates the emergence of a topological semimetal phase at low temperatures in S35, and more in general in the shaded pink, i.e., high-mobility, composition regime in Fig. 2.

In conclusion, we have established a highly tunable PbTe-SnTe (In-doped) binary system, where carrier density and bulk polar properties are sensitively dependent on the In doping level as well as the Pb/Sn ratio. Over a finite composition range at ambient pressure, this system manifests itself as a topological semimetal phase with a magnetic-field-induced Berry curvature inducing a large anomalous Hall effect, accompanied by inversion symmetry breaking as revealed by

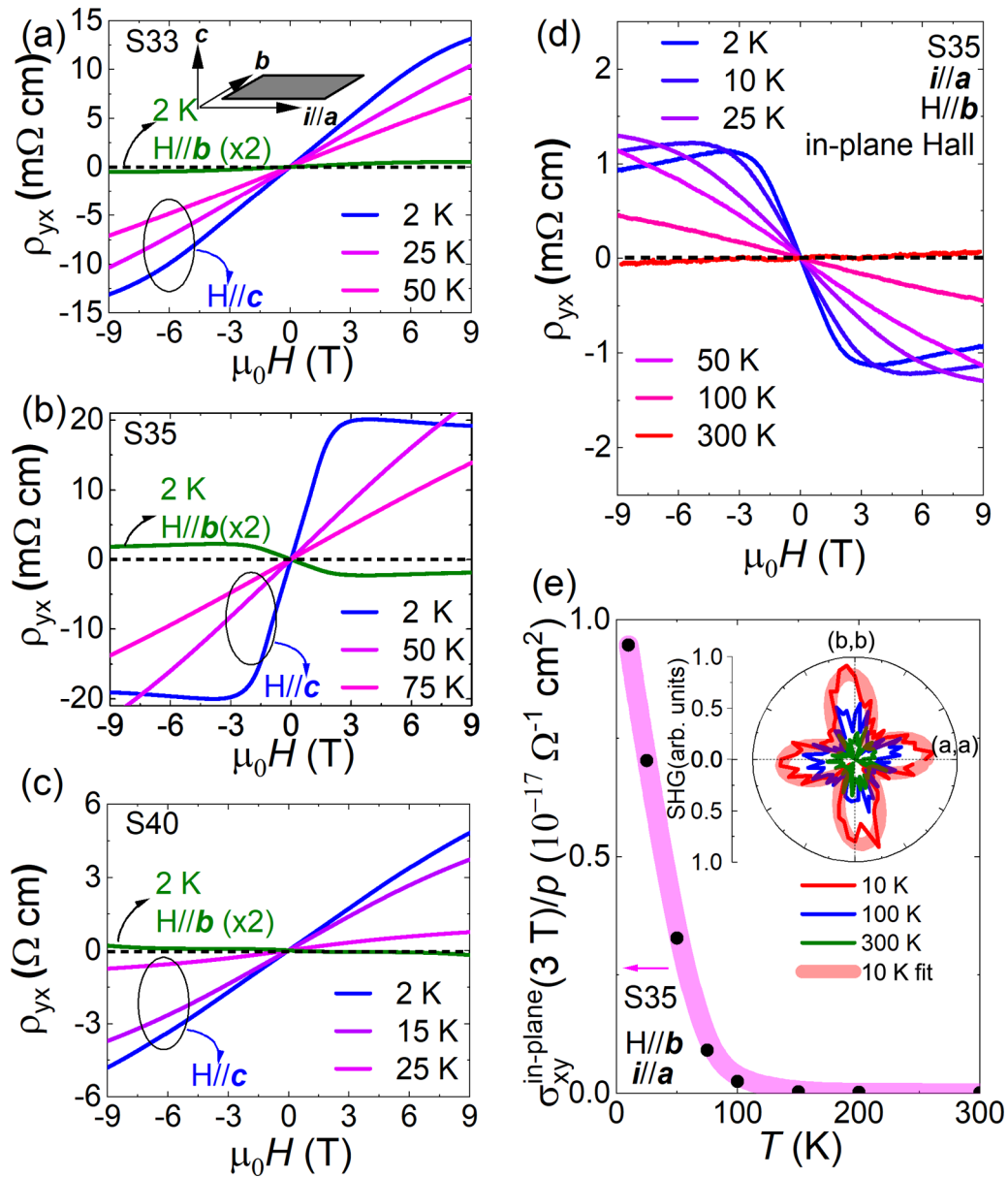


FIG. 4. In-plane anomalous Hall effect as a signature of Berry curvature of the topological semimetal candidate crystal. (a)–(c) Out-of-plane ( $H||c$ ) and in-plane ( $H||b$ ) Hall effects of sample S33, S35, and S40, respectively. The inset in panel (a) shows the applied current and magnetic field configuration. Only sample S35 exhibits simultaneously an obvious out-of-plane and in-plane anomalous Hall signal at 2 K. (d) Temperature dependence of the in-plane ( $H||b$ ) anomalous Hall effect for sample S35. (e) Temperature dependence of the ratio of the in-plane Hall conductivity to carrier concentration,  $\sigma_{xy}^{\text{in-plane}}(3 \text{ T})/\rho$ , for sample S35. This quantity is predicted to be proportional to the Berry curvature  $\langle \Omega_z \rangle$ , see Eq. (1), showing a large enhancement below 100 K. The inset shows temperature dependent polar plots of the second harmonic generation (SHG) signal with normal incident fundamental laser light (1.5 eV with pulse duration of 120 fs) on the  $ab$  plane of S35, indicating the polarity generation along the  $\langle 100 \rangle$  axes. The thick pink line is a guide to the eyes.

SHG measurements. The emergence of such a highly tunable system provides an ideal material platform for further investigating the versatile nature of topological semimetal phases in forthcoming studies from a wide perspective.

We thank M. S. Bahramy, M. Hirayama, M. Kawasaki, and N. Nagaosa for helpful discussions. This project was partly supported by CREST (Grant No. JPMJCR16F1) from JST. N.O. is supported by PRESTO JST (No. JPMJPR17I3).

[1] D. Thouless, M. Kohmoto, M. Nightingale, and M. Den Nijs, Quantized Hall Conductance in a Two-Dimensional Periodic Potential, *Phys. Rev. Lett.* **49**, 405 (1982).

[2] C. L. Kane and E. J. Mele, Quantum Spin Hall Effect in Graphene, *Phys. Rev. Lett.* **95**, 226801 (2005).

- [3] C. L. Kane and E. J. Mele, Z<sub>2</sub> Topological Order and the Quantum Spin Hall Effect, *Phys. Rev. Lett.* **95**, 146802 (2005).
- [4] B. Bernevig and S.-C. Zhang, Quantum Spin Hall Effect, *Phys. Rev. Lett.* **96**, 106802 (2006).
- [5] M. Z. Hasan and C. L. Kane, Colloquium: Topological insulators, *Rev. Mod. Phys.* **82**, 3045 (2010).
- [6] Z. Wang, Y. Sun, X.-Q. Chen, C. Franchini, G. Xu, H. Weng, X. Dai, and Z. Fang, Dirac semimetal and topological phase transitions in A<sub>3</sub>Bi (A = Na, K, Rb), *Phys. Rev. B* **85**, 195320 (2012).
- [7] Z. Wang, H. Weng, Q. Wu, X. Dai, and Z. Fang, Three-dimensional Dirac semimetal and quantum transport in Cd<sub>3</sub>As<sub>2</sub>, *Phys. Rev. B* **88**, 125427 (2013).
- [8] S.-M. Huang, S.-Y. Xu, I. Belopolski, C.-C. Lee, G. Chang, B. Wang, N. Alidoust, G. Bian, M. Neupane, and C.-L. Zhang *et al.* A Weyl fermion semimetal with surface fermi arcs in the transition metal monophosphide TaAs class, *Nat. Commun.* **6**, 7373 (2015).
- [9] H. Weng, C. Fang, Z. Fang, B. A. Bernevig, and X. Dai, Weyl Semimetal Phase in Noncentrosymmetric Transition-Metal Monophosphides, *Phys. Rev. X* **5**, 011029 (2015).
- [10] B. Bradlyn, L. Elcoro, J. Cano, M. Vergniory, Z. Wang, C. Felser, M. Aroyo, and B. Bernevig, Topological quantum chemistry, *Nature (London)* **547**, 298 (2017).
- [11] H. Po, A. Vishwanath, and H. Watanabe, Symmetry-based indicators of band topology in the 230 space groups, *Nat. Commun.* **8**, 50 (2017).
- [12] F. Tang, H. Po, A. Vishwanath, and X. Wan, Comprehensive search for topological materials using symmetry indicators, *Nature (London)* **566**, 486 (2019).
- [13] T. Zhang, Y. Jiang, Z. Song, H. Huang, Y. He, Z. Fang, H. Weng, and C. Fang, Catalogue of topological electronic materials, *Nature (London)* **566**, 475 (2019).
- [14] M. Vergniory, L. Elcoro, C. Felser, N. Regnault, B. Bernevig, and Z. Wang, A complete catalogue of high-quality topological materials, *Nature (London)* **566**, 480 (2019).
- [15] S. Murakami, Phase transition between the quantum spin Hall and insulator phases in 3D: Emergence of a topological gapless phase, *New J. Phys.* **9**, 356 (2007).
- [16] S. Murakami and S. Kuga, Universal phase diagrams for the quantum spin Hall systems, *Phys. Rev. B* **78**, 165313 (2008).
- [17] R. Okugawa and S. Murakami, Dispersion of Fermi arcs in Weyl semimetals and their evolutions to Dirac cones, *Phys. Rev. B* **89**, 235315 (2014).
- [18] B.-J. Yang and N. Nagaosa, Classification of stable three-dimensional Dirac semimetals with nontrivial topology, *Nat. Commun.* **5**, 4898 (2014).
- [19] S. Murakami, M. Hirayama, R. Okugawa, and T. Miyake, Emergence of topological semimetals in gap closing in semiconductors without inversion symmetry, *Sci. Adv.* **3**, e1602680 (2017).
- [20] B. Bernevig, T. Hughes, and S.-C. Zhang, Quantum spin Hall effect and topological phase transition in HgTe quantum wells, *Science* **314**, 1757 (2006).
- [21] M. König, S. Wiedmann, C. Brune, A. Roth, H. Buhmann, L. Molenkamp, X.-L. Qi, and S.-C. Zhang, Quantum spin Hall insulator state in HgTe quantum wells, *Science* **318**, 766 (2007).
- [22] K. L. I. Kobayashi, Y. Kato, Y. Katayama, and K. F. Komatsubara, Carrier-Concentration-Dependent Phase Transition in SnTe, *Phys. Rev. Lett.* **37**, 772 (1976).
- [23] T. Shimada, K. L. I. Kobayashi, Y. Katayama, and K. F. Komatsubara, Soft-Phonon-Induced Raman Scattering in IV-VI Compounds, *Phys. Rev. Lett.* **39**, 143 (1977).
- [24] Y. Tanaka, Z. Ren, T. Sato, K. Nakayama, S. Souma, T. Takahashi, K. Segawa, and Y. Ando, Experimental realization of a topological crystalline insulator in SnTe, *Nat. Phys.* **8**, 800 (2012).
- [25] S.-Y. Xu, C. Liu, N. Alidoust, M. Neupane, D. Qian, I. Belopolski, J. Denlinger, Y.-J. Wang, H. Lin, and L. Wray *et al.*, Observation of a topological crystalline insulator phase and topological phase transition in Pb<sub>1-x</sub>Sn<sub>x</sub>Te, *Nat. Commun.* **3**, 1192 (2012).
- [26] R. Zhong, J. Schneeloch, Q. Li, W. Ku, J. Tranquada, and G. Gu, Indium substitution effect on the topological crystalline insulator family (Pb<sub>1-x</sub>Sn<sub>x</sub>)<sub>1-y</sub>In<sub>y</sub>Te: Topological and superconducting properties, *Crystals* **7**, 55 (2017).
- [27] T. Liang, S. Kushwaha, J. Kim, Q. Gibson, J. Lin, N. Kioussis, R. Cava, and N. P. Ong, A pressure-induced topological phase with large berry curvature in Pb<sub>1-x</sub>Sn<sub>x</sub>Te, *Sci. Adv.* **3**, e1602510 (2017).
- [28] L. Fu, Topological Crystalline Insulators, *Phys. Rev. Lett.* **106**, 106802 (2011).
- [29] T. Hsieh, H. Lin, J. Liu, W. Duan, A. Bansil, and L. Fu, Topological crystalline insulators in the SnTe material class, *Nat. Commun.* **3**, 982 (2012).
- [30] P. Dziawa, B. J. Kowalski, K. Dybko, R. Buczko, A. Szczerbakow, M. Szot, E. Lusakowska, T. Balasubramanian, B. Wojek, and M. H. Berntsen *et al.*, Topological crystalline insulator states in Pb<sub>1-x</sub>Sn<sub>x</sub>Se, *Nat. Mater.* **11**, 1023 (2012).
- [31] See Supplemental Material at <http://link.aps.org/supplemental/10.1103/PhysRevMaterials.4.091201> for details on sample characterizations, zero-angle correction, concentration distribution in other Bridgman rods, and anomalous Hall effect in another sample.
- [32] M. Kriener, M. Sakano, M. Kamitani, M. S. Bahramy, R. Yukawa, K. Horiba, H. Kumigashira, K. Ishizaka, Y. Tokura, and Y. Taguchi, Evolution of Electronic States and Emergence of Superconductivity in the Polar Semiconductor GeTe by Doping Valence-Skipping Indium, *Phys. Rev. Lett.* **124**, 047002 (2020).
- [33] N. Haldolaarachchige, Q. Gibson, W. Xie, M. B. Nielsen, S. Kushwaha, and R. J. Cava, Unusual nature of fully gapped superconductivity in In-doped SnTe, *Phys. Rev. B* **93**, 024520 (2016).
- [34] M. Kriener, M. Kamitani, T. Koretsune, R. Arita, Y. Taguchi, and Y. Tokura, Tailoring band structure and band filling in a simple cubic (IV, III)-VI superconductor, *Phys. Rev. Mater.* **2**, 044802 (2018).
- [35] N. Romević, Z. V. Popović, D. Khokhlov, A. V. Nikorich, and W. König, Far-infrared study of localized states in In-doped Pb<sub>0.75</sub>Sn<sub>0.25</sub>Te single crystals, *Phys. Rev. B* **43**, 6712 (1991).
- [36] B. A. Akimov, A. V. Dmitriev, D. R. Khokhlov, and L. I. Ryabova, Carrier transport and non-equilibrium phenomena in doped PbTe and related materials, *Phys. Stat. Solidi A* **137**, 9 (1993).

- [37] S. Takaoka, T. Itoga, and K. Murase, Investigation of transport properties in  $\text{Pb}_{1-x}\text{Sn}_x\text{Te}$  doped with indium, *Jpn. J. Appl. Phys.* **23**, 216 (1984).
- [38] C. O'Neill, D. Sokolov, A. Hermann, A. Bossak, C. Stock, and A. Huxley, Inelastic x-ray investigation of the ferroelectric transition in SnTe, *Phys. Rev. B* **95**, 144101 (2017).
- [39] T. Liang, J. Lin, Q. Gibson, S. Kushwaha, M. Liu, W. Wang, H. Xiong, J. A. Sobota, M. Hashimoto, P. S. Kirchmann *et al.*, Anomalous Hall effect in  $\text{ZrTe}_5$ , *Nat. Phys.* **14**, 451 (2018).